Journal of Computational Electronics
https://doi.org/10.1007/s10825-022-01942-5

Numerical study of high-efficiency CIGS solar cells by inserting a BSF µc-Si:H layer

Rafik Zouache[1] · Idris Bouchama[1,2] · Okba Saidani[3] · Layachi Djedoui[4] · Elyazid Zaidi[5]

Received: 17 July 2022 / Accepted: 24 August 2022

Abstract
In this paper, we present a simulation study of Cu(In,Ga)Se_2 (CIGS) based solar cell using a physically based two-dimensional device simulator Silvaco-Atlas under AM1.5 illumination. First, we studied the effect of CIGS layer thickness, doping concentrations, and defects on the J–V properties and the quantum efficiency (QE) of a conventional cell. The simulated structure shows an open circuit voltage equal to 0.80 V, a short circuit current density equal to 30.03 mA/cm^2, a fill factor equal to 82.77% and the obtained efficiency of the conventional cell is 19.80% with CIGS absorber layer thickness of about 1.5 µm, our simulation results of the CIGS solar cell are in good agreement with the simulated and experimental results found in literature. In order to improve the solar cells efficiency, the back surface field (BSF) based on hydrogenated microcrystalline silicon µc-Si:H(p+) layer has been inserted between the back contact (Mo) and the CIGS absorber layer, in this case the structure presents an open voltage equal to 0.84 V, a short circuit current density equal to 32.55 mA/cm^2, a fill factor equal to 85.31% and an efficiency of 23.42%. The obtained results demonstrate that the addition of µc-Si:H(p+) BSF layer increases the efficiency of CIGS solar cells, reaching a maximum value of 23.42% for 1.5 µm of CIGS thickness and 10 nm for µc-Si:H(p+) BSF layer.

Keywords Solar cells · CIGS · Efficiency · Back surface field · µc-Si: H

1 Introduction

Over the past several years, thin film solar cells have gained increased attention due to their high efficiency and low cost [1]. Thin film solar cells may be made from a variety of materials, including Cu (In, Ga) Se (CIGS), CdTe, and CZTS [2]. Due to its high efficiency for terrestrial applications, CIGS-based solar cells are now gaining footing in the photovoltaic industry [3]. Where the material is simple to make [4], has a low manufacturing cost [5, 6] good durability and stability [7, 8], and radiation hardness [9, 10]. It also has a high optical absorption coefficient (10^5 cm^1) [11] and a tunable band-gap ranging from 1.02 eV for $CuInSe_2$ (CIS) to 1.68 eV for $CuGaSe_2$ [12–14]. These latter characteristics are among the exceptional advantages of the CIGS compound material [15–17]. In recent years, several investigations have been carried out to enhance and advance CIGS solar cells. Repins and al. suggested a 19.9% efficient in CIGS-based solar cell in 2008 [18]. In addition, Chirilă et al. published an article of ZnO: Al/i-ZnO/CdS/CIGS solar cell structure, which presents an efficiency of 20.4% [19]. In 2016, the efficiency of the conventional CIGS solar cell was improved to 22.6% by using alkali element of Potassium [11]. Very recently, efficiency up to 22.9% was announced by Kato et al. [20] in 2019 for the conventional structure achieved by Caesium treatment. By inserting new layer of p-type Si, Heriche et al. [21] improved the efficiency to 21.3% with a very thin CIGS absorber layer of about 1 µm, with a structure ZnO/CdS/CIGS/Si.

The back surface field (BSF) plays an important role in improving the device efficiency and reducing the thickness

✉ Rafik Zouache
rafik.zouache@univ-msila.dz

1 Electronics Department, Faculty of Technology, University of Msila, 28000 City of Msila, Algeria

2 Research Unit on Emerging Materials (RUEM), University of Ferhat Abbas, Setif1, City of Sétif, Algeria

3 Faculty of Science and Technology, University of Biskra, City of Biskra, Algeria

4 Faculty of Technology, University of Saad Dahlab Blida.1, City of Blida, Algeria

5 Polytechnic Military School, Bordj El-Bahri, City of Algiers, Algeria

Published online: 09 September 2022

of the absorbers layers [22–24]. The hydrogenated microcrystalline silicon (μc-Si:H) layer used as BSF can raise the conversion efficiency more than 4% compared to a solar cell without BSF layer [25].

In this work, we have used the Silvaco-Atlas software on the design and the study of structure of CIGS thin film solar cells structure. Firstly, we studied the effect of CIGS layer thickness, doping concentrations, and defects on the J–V properties and the quantum efficiency (QE) of a conventional cell ZnO/CdS/CIGS. In the second step, we will show that the simulation results of the device performance are affected by adding the back surface field using μc-Si:H BSF layer. We also studied the effect of defect density on the performance of substrate ZnO/CdS/CIGS/ μc-Si:H solar cells structure.

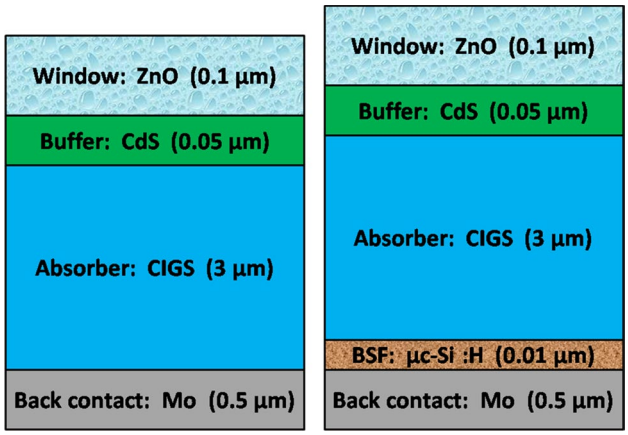

Fig. 1 The CIGS cell structure with and without BSF layer

2 Device structure and simulation

In the conventional structure, the n-type CdS buffer layer is inserted between the ZnO window layer and *p*-type CIGS absorber layer to make a high quality *p–n* junction in the interface [26]. In the proposed structure, we have inserted a BSF layer based on μc-Si:H between the back contact Molybdenum (Mo) and the CIGS absorber layer. The CIGS is a p-type semiconductor with 3 μm-thick and 2×10^{16} cm^{-3}acceptor density [27] with a moderate gap $E_g = 1.3$ eV [28]. The n-type CdS buffer layer was taken using 50 nm-thick and 2×10^{18} cm^{-3}donor density with a gap of 2.4 eV. The degenerate ZnO(n+) window layer was taken as a wide band-gap the transparent conducting oxide (TCO) semiconductor (3.30 eV), with 100 nm-thick and 1×10^{19} cm^{-3} as a donor density [29]. In the proposed structure, a very thin back surface field (BSF) μc-Si:H(p+) of 10 nm-thick, and heavily doped with 1×10^{21} cm^{-3} hole density and band-gap of 1.45 eV [25]. A schematic view of the conventional CIGS solar cell structure and the new structure with a BSF layer are displayed in Fig. 1

The simulations were performed using the 2D and 3D computer simulator Atlas-Silvaco. It predicts the electrical behavior of specified semiconductor structures and provides insight into the internal physical mechanisms associated with device operation. The Atlas-Silvaco simulator allows the solution of a set of basic semiconductor equations consisting of the Poisson equation and the continuity and transport equations for electrons and holes [30].

The band-gap E_g of the semiconductors Cu $(In_{(1-x)}, Ga_x)$ Se_2 alloys was calculated using the following expression [31].

$$E_g[\text{eV}] = 1.010 + 0.626 \cdot x - 0.167 \cdot x(1-x) \tag{1}$$

where E_g ranges from 1.011 to 1.69 eV for x ranging from 0 for CIS to 1 for CGS, respectively.

The input parameters of each layer of the proposed structure are summarized in Table 1. These parameters are the thickness w, the permittivity constant εr, the band-gap E_g, the electron affinity χ_e, the electron/hole mobility μ_n/μ_p, the effective density of states in conduction/valence band N_C/N_V, and the donor/acceptor concentration N_D/N_A. At the front contact, the reflection was neglected. The values of the surface recombination velocity for holes/electrons S_n/S_p at front and back contacts were 1×10^7 cm/s.

Because all of the layers are polycrystalline, they include a wide range of defects [18]. Therefore, for the (CIGS/μc-Si:H) layers, we used a tow Gaussian deep donor defect distribution, and tow Gaussian deep acceptor defect distribution for the (ZnO/CdS) layers. The donor and acceptor defect distributions are provided by Atlas [30, 31].

$$g_{GA}(E) = N_{GA}\exp\left[-\left[\frac{E_{GA}-E}{W_{GA}}\right]^2\right] \tag{2}$$

$$g_{GD}(E) = N_{GD}\exp\left[-\left[\frac{E-E_{GD}}{W_{GD}}\right]^2\right] \tag{3}$$

where E is the defect energy, the subscripts (G, A, D) stand for Gaussian acceptor and donor defect states, respectively. The effective density of states (N_{GA} and N_{GD}), standard energy deviation (W_{GA} and W_{GD}), and peak energy position all characterize the density of states (E_{GA} and E_{GD}). In this study, the solar cells operating temperature was set at 300 K.

Table 1 Physical parameters and defect state for materials used in the simulation

Parameter	ZnO (n)	CdS (n)	CIGS (p)	µc-Si:H (p+)
Thickness w (µm)	0.1	0.05 [32]	3*	0.01 [25]
Band gap energy E_g (eV)	3.3 [21]	2.4 [31]	1.3 [28]	1.45 [25]
Doping density N_D/N_A (cm^{-3})	1×10^{19}	2×10^{18} [28]	2×10^{16}*	1×10^{21}*
Electron affinity χ_e (eV)	4.6 [23]	4.2[23]	4.5 [21]	4 [25]
Relative permittivity ε_r (F cm^{-1})	9 [22]	10 [31]	13.6 [4]	11.9 [25]
Density of states at conduction band N_C (cm^{-3})	2.2×10^{18} [32]	2.2×10^{18} [31]	2.2×10^{18} [4]	10^{19} [25]
Density of states at valence band N_V (cm^{-3})	1.8×10^{19} [22]	1.8×10^{19} [32]	1.8×10^{19} [4]	10^{19} [25]
Electron mobility μ_n (cm^2/Vs)	100 [31]	100 [21]	100 [31]	50 [25]
Hole mobility μ_p (cm^2/Vs)	25 [28]	25[22]	25 [23]	5 [25]
Gaussian defect density N_{GA}, N_{GD} (cm^{-3})	10^{14} (A) [21]	10^{14} (A) [21]	10^{14} (D)*	10^{14} (D)
Defect energy position E_{GA}, E_{GD} (eV)	Mid-gap■ [31]	Mid-gap■ [31]	Mid-gap■ [31]	Mid-gap■
Standard energy deviation W_{GA}, W_{GD} (eV)	0.1(A) [32]	0.1(A) [31]	0.1(D) [31]	0.1(D)
Electron capture cross section σ_n (cm^2)	10^{-12} [28]	10^{-17} [28]	10^{-13} [28]	10^{-12}
Hole capture cross section σ_p (cm^2)	10^{-15} [28]	10^{-12} [28]	10^{-15} [28]	10^{-14}
Surface recombination velocity for electrons S_n and holes S_p (cm s^{-1})				
At front contact		10^7 [32]		10^7 [32]
At CdS/CIGS interface		10^5 [31]		10^5 [31]
At back contact		10^7 [32]		10^7 [32]

■Mid-gap is the middle of the band gap

*A variable field

(A) denote Acceptor defects

(D) denote Donor defects

3 Results and discussion

Understanding the behavior and dependability of any semiconductor device depends on the band diagram derived from such a configuration [33]. The band diagram of the simulated structure in this investigation was produced using Tonyplot from Silvaco-Atlas. The obtained band diagram is displayed in Fig. 2. A good band alignment was obtained between CIGS absorber layer and the µc-Si:H back surface field. After introducing the thin µc-Si:H BSF layer, an upward facing slope is created toward the surface so that the electrons are repelled from going near the surface as seen in Fig. 2. The created back-side built-in electric field opposes minority carrier travel to the back surface, which has a high recombination velocity; hence electrons are reflected away from the back surface, minimizing rear surface recombination.

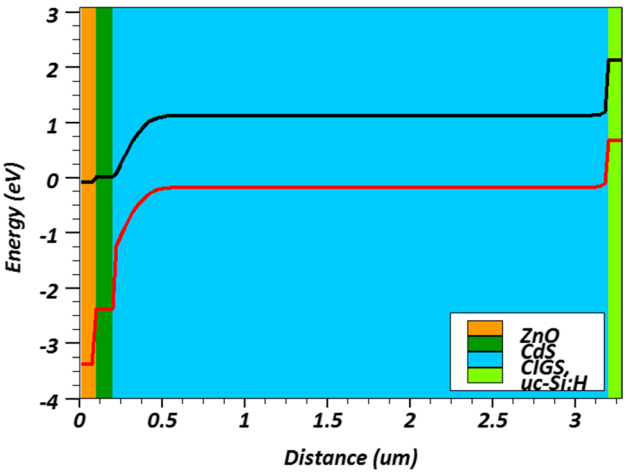

Fig. 2 Band diagram for the CIGS solar cell with BSF

3.1 Thickness optimization of CIGS absorber layer

In this part, we'll look at the performance of the ZnO/CdS/CIGS solar cell using the variables listed in Table 1, in order to estimate the optimum of CIGS absorber layer thickness. Figure 3 shows the evolution patterns of V_{oc}, J_{sc}, FF and η of ZnO/CdS/CIGS solar cell as a function of p-CIGS absorber layer thickness from 0.5 to 10 µm. When the CIGS layer thickness w(CIGS) is increased from 0.5 to 5 µm, J_{sc} rise significantly from 24 mA/cm^2 to approximately 33.95 mA/cm^2 and η increases rapidly from 14.37% to about 23.39% (by 40.17%), respectively. V_{oc} up to (0.84 V) and FF (83%), on the other hand, remain nearly unaltered. All photovoltaic properties are nearly identical for a thick p-CIGS absorber layer (more than 5 µm). This overall behavior is resulted

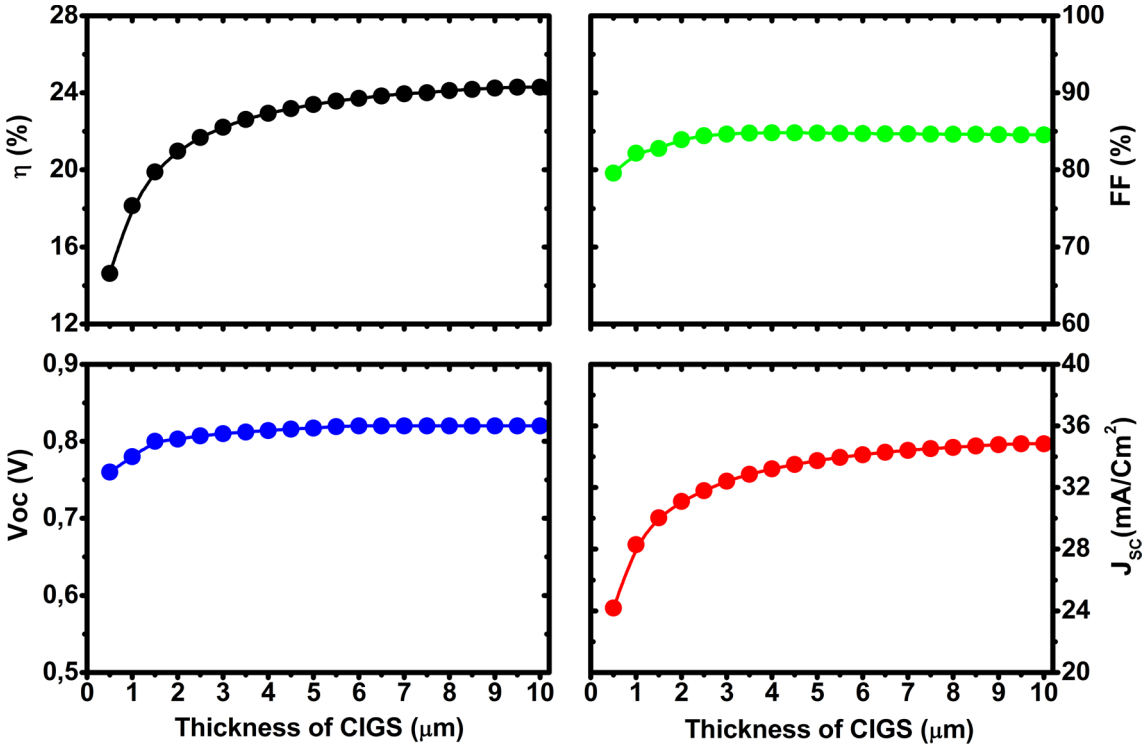

Fig. 3 Cell performances with variable thickness of CIGS absorber layer

from the increase of the photons absorption and even the increase of the electron–hole generation in the p-CIGS absorber layer. Therefore, the thickness of 5 μm is chosen as an optimum thickness for p-CIGS absorber layer for an efficient ZnO/CdS/CIGS solar cell [28]. If the absorber layer thickness is reduced the back contact will be very close to the depletion region [34]. Additionally, for comparison, similar behaviors of the performance parameters were achieved by Benmir and Heriche [35, 36].

3.2 Optimization of the acceptor density N_A (CIGS)

The acceptor concentration of the CIGS layer has been discovered to be significant factors that have a direct impact on the performance of CIGS based solar cells. As a result, the absorber layer's acceptor concentration, N_A (CIGS), is adjusted from 10^{12} to 10^{18} cm^{-3}, and the simulated photovoltaic characteristics are displayed in Fig. 4. The J_{sc} exhibits a very modest drop from 34,08 mA/cm^2 for a concentration of 10^{14} cm^{-3} to an acceptable limit of 31,55 mA/cm^2 for a concentration of 4×10^{17} cm^{-3}, which is caused by an increase in free carrier charge recombination that occurs inside the bulk [37]. On the other hand, V_{oc}, FF and efficiency are increased significantly with the increase of N_A (CIGS) from 10^{12} to 10^{17} cm^{-3} whereas the optimum efficiency achieved is 22.49% in the acceptor concentration of about 10^{17} cm^{-3}, the $V_{oc} \approx 0.83$ V and FF ≈84.37%. After this value the structure presents a strong decrease in the V_{oc} FF and efficiency. The result indicates that the N_A (CIGS) must be higher than 10^{16} cm^{-3} and lower than 10^{17} cm^{-3} to obtain a good performance.

3.3 Influence defect state density of CIGS absorber layer N_G (CIGS)

The conversion efficiency of CIGS-based solar cells is drastically reduced when defects caused by increased Ga content are considered. The simulation results of CIGS solar cell with various Gaussian defect state densities positioned in the CIGS bulk band-gap N_G (CIGS) are presented in Fig. 5. When N_G (CIGS) > 10^{15} cm^{-3}, the figure depicts a negative influence on the device's performance. All the photovoltaic parameters, including V_{oc}, J_{sc}, FF, and η, are reduced. Charge carriers become trapped or recombined in flaws, resulting in a waste of energy that does not contribute to the transportation of current to the external load. When N_G (CIGS) 10^{14} cm^{-3}, the greatest attainable values of photovoltaic parameters were reached. $J_{sc} = 32.41$ mA/cm^2, $V_{oc} = 0.81$ V, FF = 84.65%, and $\eta = 22.21\%$ were the highest obtained parameters at N_G (CIGS) = 10^{14} cm^{-3}. The J–V characteristics were reduced due to a defect concentration of around 3×10^{18} cm^{-3}, with $J_{sc} = 18.95$ mA/cm^2, $V_{oc} = 0.57$ V, FF = 22.1%, and $\eta = 2.4\%$. Because of the high recombination rate, this deterioration occurs. As a result,

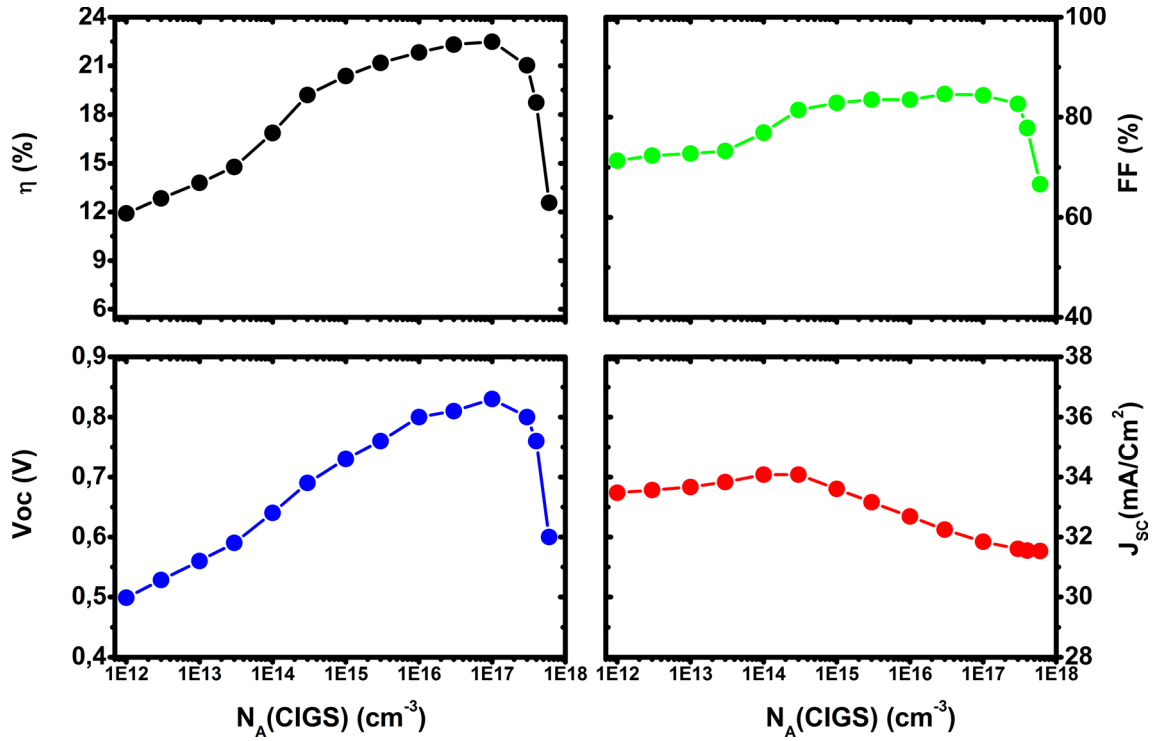

Fig. 4 Effect of acceptor concentration of absorber layer N_A (CIGS) on cell performances

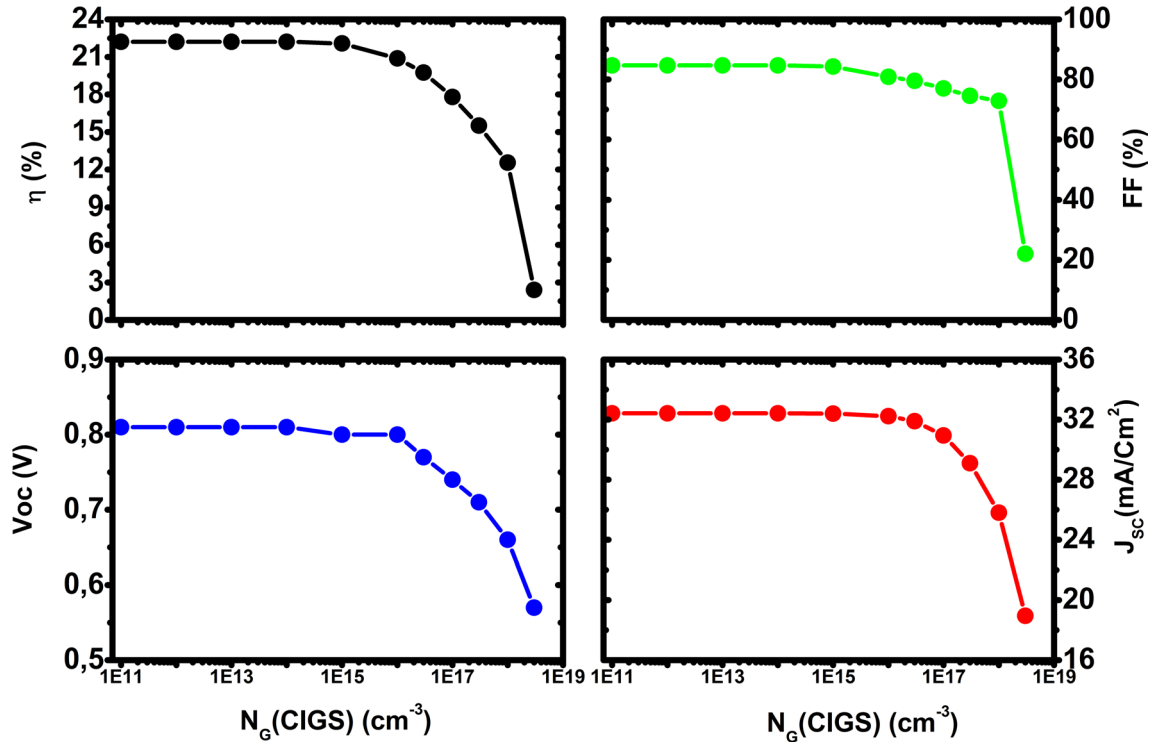

Fig. 5 Parameters of the basic solar cell as a function of Gaussian defects concentration N_G (CIGS)

the bulk defect density, which is connected to creating trapping (recombination state) in the absorber bulk, may have a significant impact on current transport [38].

3.4 Performance optimization of CIGS layer for the new structure

In Fig. 6, the quantum efficiency (QE) of the solar cell structure ZnO/CdS/CIGS/μc-Si:H(p+)/Mo with various CIGS layer thicknesses is shown. We can see that QE increases as the CIGS layer thickness increases. This is because as the thickness of the absorber layer increases, more photons are absorbed [39].

The simulation results for conventional solar cells and solar cells with BSF layer are given in Fig. 7, which was achieved by adding 10 nm of the new layer μc-Si:H to the simulation results for conventional solar cells and solar cells with BSF layer. We can see in Fig. 3 that the optimum thickness was in the range of 5 μm, which corresponds to an efficiency of 23.39% in the conventional cell; however, using a cell with BSF, the new optimum thickness of 1.5 μm achieves an efficiency of 23.42%. Note that the electric efficiency increases rapidly in the cell with BSF; it is noteworthy that the efficiency has jumped from 18.6 to 22.08% for the 0.5 μm and 1 μm, respectively. This is owing to the fact that the majority of electron/hole pairs are created when the absorber layer is bulky. Given the high cost of gallium and indium materials in CIGS solar cells [40, 41], lowering the usage of indium and gallium materials by reducing the layer thickness is sufficient to minimize the cost of CIGS cell manufacture. Furthermore, by inserting the BSF between CIGS and Mo, it is feasible to enhance the efficiency of the cell with a thin layer of CIGS, which is advantageous since it saves money and time in the CIGS solar cell production.

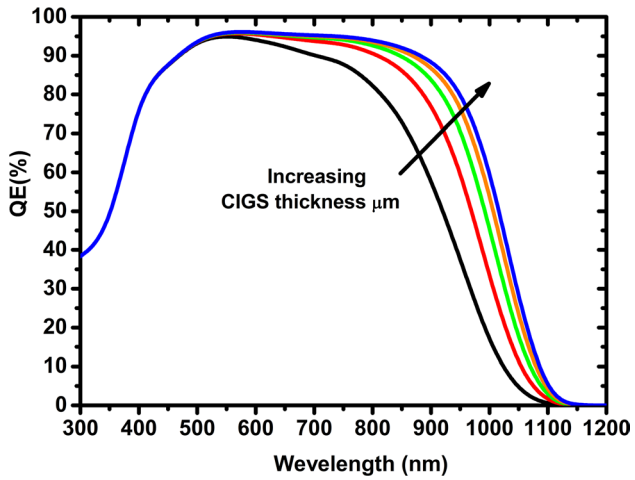

Fig. 6 Quantum efficiency for the cell structure with BSF layer

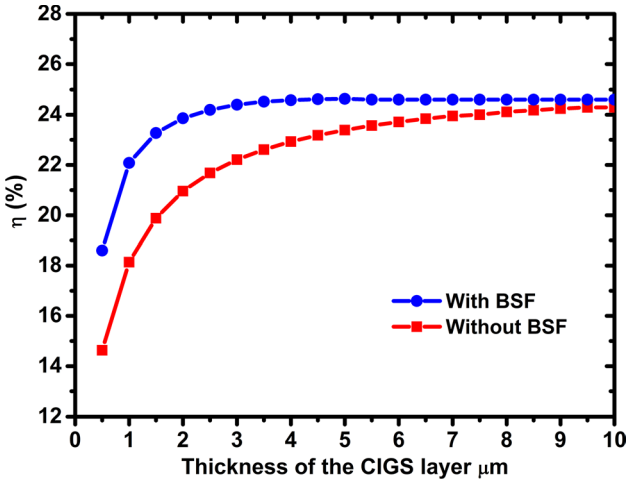

Fig. 7 Performance of efficiency with variable thickness of CIGS layer for the conventional structure and modified cell with the BSF layer

In Fig. 8, we found that the cell with BSF layer exhibited better J–V characteristics. Indeed, from this plot, it is clear that the cell with BSF possesses better performances comparing to the basic cell; in Table 2, the main results are displayed. According to this table, it is evident that all these parameters are improved by the insertion of the BSF layer.

3.5 Influence of acceptor density of BSF layer on cell performance

The influence of BSF doping level on cell performance is seen in Fig. 9. The concentration of the μc-Si:H layer was varied from 10^{13} to 10^{21} cm^{-3}, and we noticed that the photovoltaic parameters the efficiency and the open

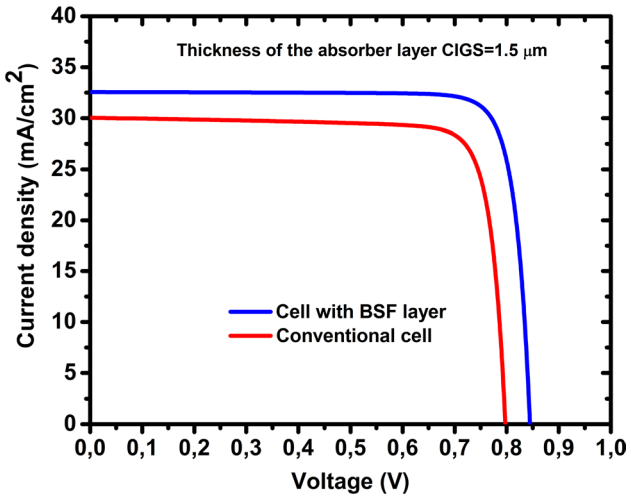

Fig. 8 J–V characteristics for CIGS solar cell with and without BSF layer

Table 2 The influence of BSF µc-Si: H layer in comparison with similar research and compared with other reported CIGS solar cells

No	Type of research	CIGS (nm) thickness	J_{sc} (mA/cm^2)	V_{oc} (V)	FF (%)	η (%)	References
1	Experimental	2500	38.50	0.74	79.70	22.92	[20]
2	Experimental	1000	35.71	0.69	78.12	19.20	[43]
3	Experimental	2200	35.50	0.69	81.20	19.90	[18]
4	Theoretical	2000	38.90	0.74	79.68	22.94	[28]
5	Theoretical	3000	33.50	0.78	82.00	21.32	[34]
6	Theoretical	1000	34.47	0.74	83.09	21.30	[21]
7	Theoretical	3500	44.39	0.65	77.49	22.69	[42]
8	Theoretical	1500	32.55	0.84	85.31	23.42	[●]
No.	Type of research	Absorber layer	BSF layer	η without BSF (%)	η with BSF (%)	Enhancement in η (%)	References
1	Experimental	Si	ZnS	6.40	11.02	72.19	[44]
2	Experimental	CIGS	$MoSe_2$	9.00	14.00	55.55	[45]
3	Theoretical	CdTe	SnS	17.40	21.83	25.45	[22]
4	Theoretical	CIGS	Si	16.39	21.30	29.96	[21]
5	Theoretical	CIGS	µc-Si: H	19.80	23.42	18.28	[●]

[●] Our work

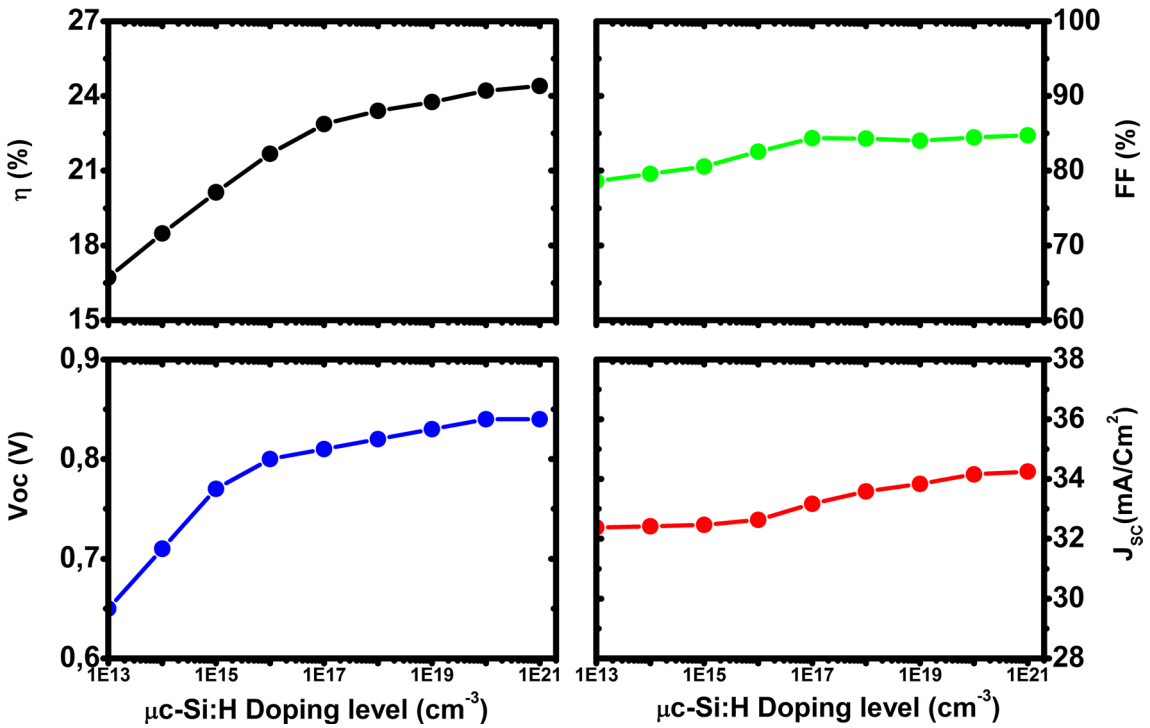

Fig. 9 Output characteristics of the solar cells versus BSF doping level

circuit voltage increase significantly as the concentration of BSF increases. This is due to the electrical field distribution at the rear contact, which prevents minority carrier recombination [23]. It can be shown that raising the BSF doping concentration from 10^{17} cm^{-3} to an acceptable limit of BSF concentration has no significant effect on the short circuit current and form factor, and that the efficiency improvement is restricted to between 23 and 24%. As a result, it can be stated that using a highly doped BSF of defining the parameters of a CIGS solar cell will be preferred.

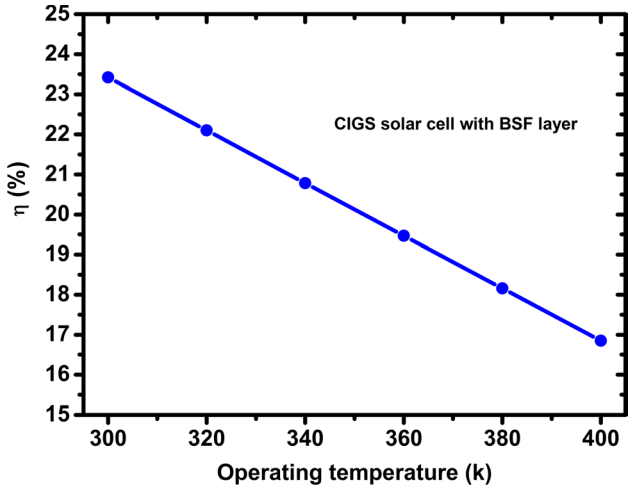

Fig. 10 Efficiency for the solar cell with BSF layer as a function of operating temperature

3.6 Effects of operating temperature on efficiency of CIGS solar cells with BSF

As illustrated in Fig. 10, lowering the temperature has a favorable and significant impact on the cell performance metrics. As the temperature drops, so does the electric efficiency. The efficiency gain is around 0.28%. At a temperature of 300 K As a result, 300 degrees Fahrenheit is the ideal temperature. Similar behaviors of performance parameters were reported in [46]. As a result, temperature is a fundamental determinant of CIGS solar cell performance; a drop in temperature boosts cell efficiency greatly. As a result, lowering the cell temperature to 300 K is preferable. Installing the cell in low-temperature areas or employing PV cell cooling methods is two ways to lower the cell temperature.

4 Conclusion

In summary, this study investigates the results of a numerical simulation of electrical properties of Cu(In,Ga)Se_2 (CIGS) based solar cell by using Silvaco-Atlas 2D numerical simulator. First, we study the effect of CIGS thickness, doping concentrations, and defects on the J–V properties and the quantum efficiency (QE) of a conventional cell. The obtained efficiency of the conventional cell is 19.80% with CIGS absorber layer thickness of about 1.5 µm, and our simulation results are in good agreement with the simulated and experimental results found in literature. The back surface field (BSF) based on hydrogenated microcrystalline silicon µc-Si:H(p+) has been introduced between the back contact (Mo) and the CIGS absorber layer in order to increase the efficiency of the solar cells. The obtained results show that the efficiency of CIGS solar cells is increased by the insertion of µc-Si:H(p+) BSF layer, And up to the value to 23.42% at 1.5 µm of CIGS thickness and 10 nm for µc-Si:H(p+) BSF layer.

Author contributions RZ: Writing—original draft, Validation, Formal analysis, Software, Writing—review & editing, Resources. IB: Investigation, Supervision, Visualization, Writing—original draft, Software. OS: Formal analysis, Software, Validation, Writing—review & editing. LD: Writing—original draft, Writing—review & editing. EZ: Writing—original draft.

Funding This work did not receive any specific give from funding agencies in the public, not for profit sectors, or commercial.

Data availability Enquiries about data availability should be directed to the authors.

Declarations

Conflict of interest The authors announced that there is no conflict of interests regarding the publication of this article.

References

1. Guirdjebaye, N., Teyou Ngoupo, A., Ouedraogo, S., Mbopda Tcheum, G.L., Ndjakan, J.M.B.: Numerical analysis of CdS-CIGS interface configuration on the performances of Cu(In, Ga)Se_2 solar cells. Chin. J. Phys. **67**, 230–237 (2020). https://doi.org/10.1016/j.cjph.2020.02.033
2. Luque, A., Hegedus, S.: Photovoltaic Science and Engineering. https://doi.org/10.1002/0470014008.
3. Ghorbani, E., Kiss, J., Mirhosseini, H., Roma, G., Schmidt, M., Windeln, J., Kühne, T.D., Felser C, C.: Hybrid-functional calculations on the incorporation of Na and K impurities in to the $CuInSe_2$ and $CuIn_5Se_8$ solar-cell materials. J. Phys. Chem. C **119**(45), 25197–25203 (2015). https://doi.org/10.1021/acs.jpcc.5b07639
4. Biplab, S.R.I., Ali, M.H., Moon, M.M.A., Pervez, M.F., Rahman, M.F., Hossain, J.: Performance enhancement of CIGS-based solar cells by incorporating an ultrathin $BaSi_2$ BSF layer. J. Comput. Electron. **19**(1), 342–352 (2019). https://doi.org/10.1007/s10825-019-01433-0
5. Huang, C.H.: Effects of Ga content on Cu(In, Ga)S_e2 solar cells studied by numerical modelling. J. Phys. Chem. Solids **69**(2–3), 330–334 (2008). https://doi.org/10.1016/j.jpcs.2007.07.093
6. Wei, S.H., Zhang, S.B., Zunger, A.: Effects of Ga addition to $CuInSe_2$ on its electronic, structural, and defect properties. Appl. Phys. Lett. **72**(24), 3199–3201 (1998). https://doi.org/10.1063/1.121548
7. Gloeckler, M., Sites, J.R.: Band-gap grading in Cu (In, Ga) Se_2 solar cells. J. Phys. Chem. Solids **66**(11), 1891–1894 (2005). https://doi.org/10.1016/j.jpcs.2005.09.087
8. Friedlmeier, T.M., Jackson, P., Bauer, A., Hariskos, D., Kiowski, O., Wuerz, R., Powalla, M.: Improved photocurrent in Cu(In, Ga) Se_2 solar cells: from 20.8% to 21.7% efficiency with Cds buffer. IEEE J. Photovolt. **5**(5), 1487–1491 (2015). https://doi.org/10.1109/JPHOTOV.2015.2458039
9. Jackson, P., Wuerz, R., Hariskos, D., Lotter, E., Witte, W., Powalla, M.: Effects of heavy alkali elements in Cu (In, Ga) Se_2 solar cells with efficiencies up to 22.6%. Phys. Status Solidi

Rapid Res. Lett. **10**(8), 583–586 (2016). https://doi.org/10.1002/pssr.201600199
10. Goffard, J., Colin, C., Mollica, F., Cattoni, A., Sauvan, C., Lalanne, P., Guillemoles, J.F., Naghavi, N., Collin, S.: Light trapping in ultrathin CIGS solar cells with nanostructured back mirrors. IEEE J. Photovolt. **7**(5), 1433–1441 (2017). https://doi.org/10.1109/jphotov.2017.2726566
11. Ullal, H. S., Zwelbel, K., Von Roedern, B.: Current status of polycrystalline thin-film PV technologies. In: Conference Record of the Twenty Sixth IEEE Photovoltaic Specialists Conference-1997, pp. 301–305. IEEE. https://doi.org/10.1109/pvsc.1997.654089.
12. Yamaguchi, M.: Radiation resistance of compound semiconductor solar cells. J. Appl. Phys. **78**(3), 1476–1480 (1995). https://doi.org/10.1063/1.360236
13. Afshari, H., Durant, B.K., Brown, C.R., Hossain, K., Poplavskyy, D., Rout, B., Sellers, I.R.: The role of metastability and concentration on the performance of CIGS solar cells under low-intensity-low-temperature conditions. Sol. Energy Mater. Sol. Cells **212**, 110571 (2020). https://doi.org/10.1016/j.solmat.2020.110571
14. Ishizuka, S., Yamada, A., Fons, P., Niki, S.: Flexible Cu(In, Ga) Se_2 solar cells fabricated using alkali-silicate glass thin layers as an alkali source material. J. Renew. Sustain. Energy **1**(1), 013102 (2009). https://doi.org/10.1063/1.3005376
15. Chirilă, A., Buecheler, S., Pianezzi, F., Bloesch, P., Gretener, C., Uhl, A.R., Kranz, L., Perrenoud, J., Seyrling, S., Verma, S., Nishiwaki, S., Romanyuk, Y.E., Bilger, G., Tiwari, A.N.: Highly efficient Cu(In, Ga)S_e2 solar cells grown on flexible polymer films. Nat. Mater. **10**(11), 857–861 (2011). https://doi.org/10.1038/nmat3122
16. Kato, T.: Cu(In, Ga)(Se, $S)_2$ solar cell research in solar frontier: progress and current status. Jpn. J. Appl. Phys. **56**(4S), 04CA02 (2017). https://doi.org/10.7567/jjap.56.04ca02
17. Kazmerski, L.L., Hallerdt, M., Ireland, P.J., Mickelsen, R.A., Chen, W.S.: Optical properties and grain boundary effects in $CuInSe_2$. J. Vac. Sci. Technol. A Vac. Surf. Films **1**(2), 395–398 (1983). https://doi.org/10.1116/1.571928
18. Repins, I., Contreras, M., Romero, M., Yan, Y., Metzger, W., Li, J., Noufi, R.: Characterization of 19.9%-efficient CIGS absorbers. In: 2008 33rd IEEE Photovoltaic Specialists Conference, pp. 1–6. IEEE. https://doi.org/10.1109/pvsc.2008.4922628.
19. Chirilă, A., Reinhard, P., Pianezzi, F., Bloesch, P., Uhl, A.R., Fella, C., Kranz, L., Keller, D., Gretener, C., Hagendorfer, H., Jaeger, D., Erni, R., Nishiwaki, S., Buecheler, S.: Potassium-induced surface modification of Cu(In, Ga)Se_2 thin films for high-efficiency solar cells. Nat. Mater. **12**(12), 1107–1111 (2013). https://doi.org/10.1038/nmat3789
20. Kato, T., Wu, J., Hirai, Y., Sugimoto, H., Bermudez, V.: Record efficiency for thin-film polycrystalline solar cells up to 22.9% achieved by Cs-Treated Cu(In, Ga) (Se, S). IEEE J. Photovolt. **9**(1), 325–330 (2018). https://doi.org/10.1109/jphotov.2018.2882206
21. Heriche, H., Rouabah, Z., Bouarissa, N.: New ultra thin CIGS structure solar cells using SCAPS simulation program. Int. J. Hyd. Energy **42**(15), 9524–9532 (2017). https://doi.org/10.1016/j.ijhydene.2017.02.099
22. Benabbas, S., Rouabah, Z., Bouarissa, N., Chelali, N.: The role of back surface field SnS layer in improvement of efficiency of CdTe thin film solar cells. Optik Int. J. Light Electron Opt. **127**(15), 6210–6217 (2016). https://doi.org/10.1016/j.ijleo.2016.04.050
23. Cherouana, A., Labbani, R.: Numerical simulation of CZTS solar cell with silicon back surface field. Mater. Today Proc. **5**(5), 13795–13799 (2018). https://doi.org/10.1016/j.matpr.2018.02.020
24. Kim, S., Dao, V.A., Shin, C., Balaji, N., Yi, J.: Influence of n-Doped μc-Si: H back surface field layer with micro growth in Crystalline-amorphous silicon heterojunction solar cells. J. Nanosci. Nanotechnol. **14**(12), 9258–9262 (2014). https://doi.org/10.1166/jnn.2014.10123
25. Rawat, A., Sharma, M., Chaudhary, D., Sudhakar, S., Kumar, S.: Numerical simulations for high efficiency HIT solar cells using microcrystalline silicon as emitter and back surface field (BSF) layers. Sol. Energy **110**, 691–703 (2014). https://doi.org/10.1016/j.solener.2014.10.004
26. Ouédraogo, S., Zougmoré, F., Ndjaka, J.M.B.: Computational analysis of the effect of the surface defect layer (SDL) properties on Cu(In, Ga)Se2-based solar cell performances. J. Phys. Chem. Solids **75**(5), 688–695 (2014). https://doi.org/10.1016/j.jpcs.2014.01.010
27. Pudov, A.O., Kanevce, A., Al-Thani, H.A., Sites, J.R., Hasoon, F.S.: Secondary barriers in CdS–Cu(In_{1-x} Ga_x)Se_2 solar cells. J. Appl. Phys. **97**(6), 064901 (2005). https://doi.org/10.1063/1.1850604
28. Bouabdelli, M.W., Rogti, F., Maache, M., Rabehi, A.: Performance enhancement of CIGS thin-film solar cell. Optik **216**, 164948 (2020). https://doi.org/10.1016/j.ijleo.2020.164948
29. Wagner, S., Shay, J.L., Migliorato, P., Kasper, H.M.: $CuInSe_2$/CdS heterojunction photovoltaic detectors. Appl. Phys. Lett. **25**(8), 434–435 (1974). https://doi.org/10.1063/1.1655537
30. Software, D. S. Atlas User's Manual. 567–1000 (2016).
31. Elbar, M., Tobbeche, S.: Numerical simulation of CGS/CIGS single and tandem thin-film solar cells using the silvaco-atlas software. Energy Proc. **74**, 1220–1227 (2015). https://doi.org/10.1016/j.egypro.2015.07.766
32. Gloeckler, M., Sites, J.R., Metzger, W.K.: Grain-boundary recombination in Cu(In, Ga)Se_2 solar cells. J. Appl. Phys. **98**(11), 113704 (2005). https://doi.org/10.1063/1.2133906
33. Mutch, M.J., Pomorski, T., Bittel, B.C., Cochrane, C.J., Lenahan, P.M., Liu, X., Nemanich, R., Brockman, J., French, M., Kuhn, M., French, B., King, S.W.: Band diagram for low-k/Cu interconnects: the starting point for understanding back-end-of-line (BEOL) electrical reliability. Microelectron. Reliab. **63**, 201–213 (2016). https://doi.org/10.1016/j.microrel.2016.04.004
34. Chelvanathan, P., Hossain, M.I., Amin, N.: Performance analysis of copper–indium–gallium–diselenide (CIGS) solar cells with various buffer layers by SCAPS. Curr. Appl. Phys. **10**(3), 387–391 (2010). https://doi.org/10.1016/j.cap.2010.02.018
35. Benmir, A., Aida, M.S.: Analytical modeling and simulation of CIGS solar cells. Energy Proc. **36**, 618–627 (2013). https://doi.org/10.1016/j.egypro.2013.07.071
36. Heriche, H., Rouabah, Z., Bouarissa, N.: High-efficiency CIGS solar cells with optimization of layers thickness and doping. Optik Int. J. Light Electron Opt **127**(24), 11751–11757 (2016). https://doi.org/10.1016/j.ijleo.2016.09.071
37. Boudour, S., Bouchama, I., Bouarissa, N., Hadjab, M.: A study of CdTe solar cells using Ga-doped MgxZn1-xO buffer/TCO layers: simulation and performance analysis. J. Sci. Adv. Mater. Dev. **4**(1), 111–115 (2019). https://doi.org/10.1016/j.jsamd.2018.12.001
38. Rougieux, F.E., Sun, C., Macdonald, D.: Determining the charge states and capture mechanisms of defects in silicon through accurate recombination analyses: a review. Sol. Energy Mater. Sol. Cells **187**, 263–272 (2018). https://doi.org/10.1016/j.solmat.2018.07.029
39. Amin, N., Sopian, K., Konagai, M.: Numerical modeling of CdS/CdTe and CdS/CdTe/ZnTe solar cells as a function of CdTe thickness. Sol. Energy Mater. Sol. Cells **91**(13), 1202–1208 (2007). https://doi.org/10.1016/j.solmat.2007.04.006
40. Tanaka, K., Oonuki, M., Moritake, N., Uchiki, H.: Cu2ZnSnS4Cu2ZnSnS4 thin film solar cells prepared by non-vacuum processing. Sol. Energy Mater. Sol. Cells **93**(5), 583–587 (2009). https://doi.org/10.1016/j.solmat.2008.12.009

41. Jimbo, K., Kimura, R., Kamimura, T., Yamada, S., Maw, W.S., Araki, H., Katagiri, H.: Cu2ZnSnS4-type thin film solar cells using abundant materials. Thin Solid Films **515**(15), 5997–5999 (2007). https://doi.org/10.1016/j.tsf.2006.12.103
42. Ghorbani, T., Zahedifar, M., Moradi, M., Ghanbari, E.: Influence of affinity band gap and ambient temperature on the efficiency of CIGS solar cells. Optik **223**, 165541 (2020). https://doi.org/10.1016/j.ijleo.2020.165541
43. Ramanathan, K., Contreras, M.A., Perkins, C.L., Asher, S., Hasoon, F.S., Keane, J., Young, D., Romero, M., Metzger, W., Noufi, R., Ward, J., Duda, A.: Properties of 19.2% efficiency ZnO/CdS/CuInGaSe2 thin-film solar cells. Prog. Photovolt. Res. Appl. **5**, 4 (2003). https://doi.org/10.1002/pip.494
44. Yang, X., Chen, B., Chen, J., Zhang, Y., Liu, W., Sun, Y.: ZnS thin film functionalized as back surface field in Si solar cells. Mater. Sci. Semicond. Process. (2018). https://doi.org/10.1016/j.mssp.2017.08.011
45. Kohara, N., Nishiwaki, S., Hashimoto, Y., Negami, T., Wada, T.: Electrical properties of the Cu(In, Ga)S_e2/MoS_e2 /Mo structure. Sol. Energy Mater. Sol. Cells (2001). https://doi.org/10.1016/S0927-0248(00)00283-X
46. Fathi, M., Abderrezek, M., Djahli, F., Ayad, M.: Study of thin film solar cells in high temperature condition. Energy Proc. **74**, 1410–1417 (2015). https://doi.org/10.1016/j.egypro.2015.07.788